Comparison of actuator disc flows representing wind turbines and propellers

van Kuik, Gijs

DOI
10.1088/1742-6596/1037/2/022007

Publication date
2018

Document Version
Final published version

Published in
Journal of Physics: Conference Series

Comparison of actuator disc flows representing wind turbines and propellers

IOP Conf. Series: Journal of Physics: Conf. Series **1037** (2018) 022007 doi:10.1088/1742-6596/1037/2/022007

Comparison of actuator disc flows representing wind turbines and propellers

Gijs A.M. van Kuik

Duwind, Delft University of Technology, Kluyverweg 1, 2629HS Delft, NL

E-mail: g.a.m.vankuik@tudelft.nl

Abstract. Actuator disc theory is the basis for rotor design and analysis, valid for discs representing wind turbine rotors as well as propellers. In Froude's momentum theory swirl is absent, in Joukowsky's momentum theory this is included. The momentum theory including swirl, developed in *WES, 2:307-316,2017*, as well as potential flow calculations have been expanded to propeller discs. For the rotational speed $\Omega \rightarrow \infty$ the classical Froude results are recovered. For low values of Ω the propeller discs show an expanding instead of contracting wake, like wind turbine discs. Both flow regimes show a complete blockage of the flow for a low but non-zero Ω_{min}. For all wind turbine discs, so irrespective of Ω, the velocity in the meridian plane, $\sqrt{v_x^2 + v_r^2}$ is constant at the disc, for all propeller discs this is not.

1. Introduction

The momentum theory without swirl is valid for high λ rotors, as is shown in figure 1. The line shows the result of this momentum theory for the wind turbine mode, left, and the propeller mode, right. The vertical axis gives the induced velocity at the disc, the horizontal axis the undisturbed wind speed with respect to the disc, both made dimensionless by the induced velocity $\sqrt{T/(2\rho A)}$ at the static disc, with T the thrust, ρ the density and A the disc area. The static disc represents a rotor in hover, or propeller without forward speed in still air, so $U_0 = 0$. This representation is well known in helicopter literature like [9], as it is able to show the results for zero wind speed, but for the same reason only rarely used in wind turbine references, see e.g. [5]. The momentum theory and the numerical/experimental data match reasonably well except for the hovering rotor and the wind turbine rotor approaching the maximum thrust coefficient $C_T = -1$ (the top of the left curve). A numerical confirmation of the momentum theory without swirl for the wind energy regime has been presented in [15], which is now expanded to the propeller regime. The calculations have been done with a potential flow code described in [15]. Figure 2 shows the results, with a good correspondence of momentum theory and calculations. Note that unlike in many wind energy papers, in the present paper C_T, C_P and ΔH, being the jump in Bernoulli value across the disc, have a negative sign for wind energy flow states, as energy is extracted from the flow. For propeller flow states the sign is positive.

The momentum theory and the potential flow code have been expanded in [16] to discs generating swirl in the wind energy regime. The theory is limited to discs with a constant circulation around the disc axis, the so-called Joukowsky circulation distribution, by which also $\Delta H =$ constant, as will be shown. The present paper expands the results to the propeller domain, presenting momentum theory results as well as calculated flow details.

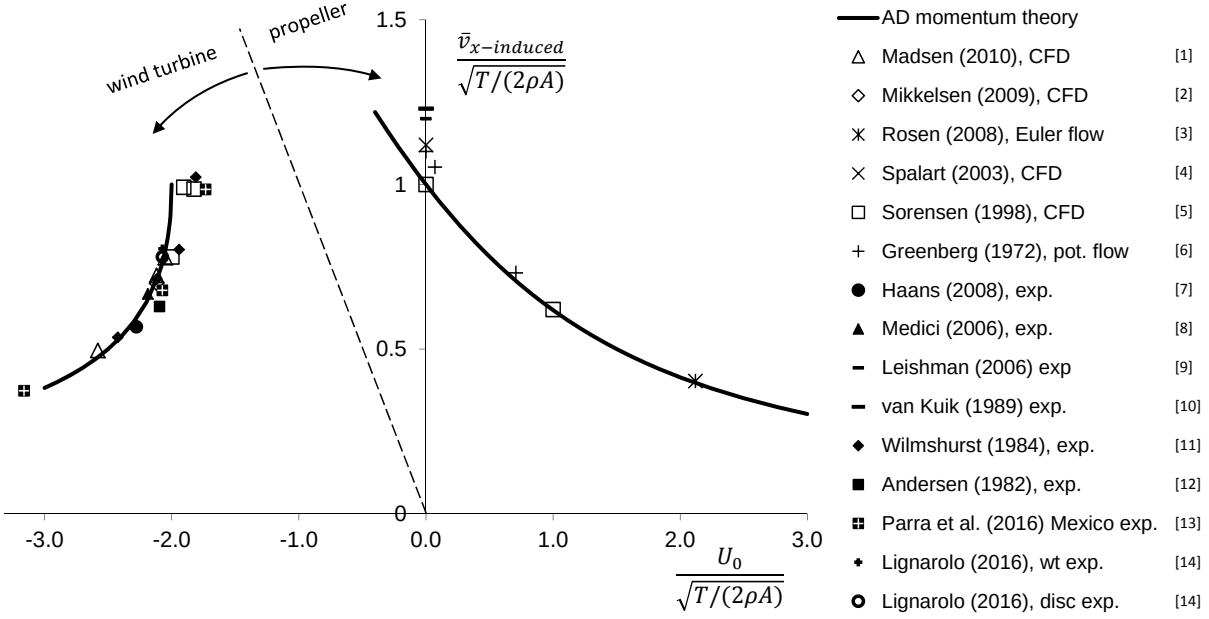

Figure 1. Actuator disc momentum theory compared with experiments and calculations. Left is the wind turbine flow regime, center and right is the propeller regime.

2. Equations of motion

The flow is governed by the steady Euler equation:

$$\rho\left(\boldsymbol{v}\cdot\boldsymbol{\nabla}\right)\boldsymbol{v}=-\boldsymbol{\nabla}p+\boldsymbol{f} \tag{1}$$

where $\boldsymbol{f}$ is the force density distributed at the disc having thickness ϵ. As only the pressure and azimuthal velocity are discontinuous for $\epsilon\to 0$, integration of (1) across the infinitely thin disc gives, in a cylindrical reference system (x,r,φ) with x pointing downstream:

$$\boldsymbol{F}=\int_{\epsilon}\boldsymbol{f}dx=\boldsymbol{e}_x\Delta p+\boldsymbol{e}_\varphi\rho v_x\Delta v_\varphi \tag{2}$$

The wake of a Joukowsky disc is characterised by a vortex Γ at the axis, having a vortex core radius δ. With $v_\varphi=\Gamma/(2\pi r)$ for $r\geq\delta$ and with the Bernoulli equation $p+\frac{1}{2}\rho\boldsymbol{v}\cdot\boldsymbol{v}=H$ integrated across the disc, the axial component is:

$$F_x=\Delta p=\Delta H-\frac{1}{2}\rho\Delta v_\varphi^2=\Delta H-\frac{1}{2}\rho\left(\frac{\Gamma}{2\pi r}\right)^2. \tag{3}$$

The power produced or absorbed by an annulus dr of the actuator disc can be expressed in two ways. First as torque Q times rotational speed Ω giving $\Omega dQ=2\pi\Omega f_\varphi r^2dr$, second by integration of $\boldsymbol{f}\cdot\boldsymbol{v}$ using (1), resulting in $2\pi r(\boldsymbol{v}.\boldsymbol{\nabla})Hdr$. Comparison shows that:

$$\boldsymbol{f}\cdot\boldsymbol{v}=\Omega r f_\varphi=(\boldsymbol{v}.\boldsymbol{\nabla})H. \tag{4}$$

The expression for rf_φ is derived from the φ-component of (1), so :

$$\Omega r f_\varphi=\rho(\boldsymbol{v}\cdot\boldsymbol{\nabla})(\Omega r v_\varphi), \tag{5}$$

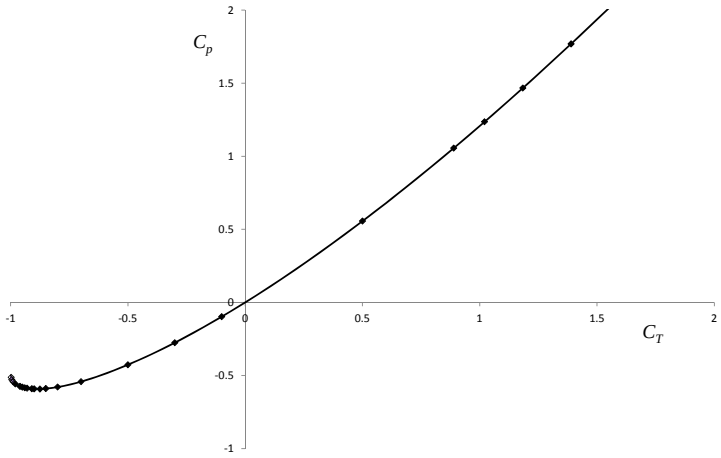

Figure 2. C_p as a function of C_T: comparison of results by the 1-D momentum theory (solid line) and potential flow calculations (♦).

and:

$$\frac{1}{\rho}\boldsymbol{\nabla}H = \boldsymbol{\nabla}\left(\Omega r v_\varphi\right) = \boldsymbol{\nabla}\left(\frac{\Omega\Gamma}{2\pi}\right). \tag{6}$$

The result is that for a Joukowsky disc

$$\Delta H = \rho\Omega\Gamma/(2\pi) = constant \tag{7}$$

Integration of (4) on disc surface A gives the converted power, in dimensionless form:

$$C_p = \frac{1}{\frac{1}{2}\rho U_0^3 A}\int_A \boldsymbol{f}\cdot\boldsymbol{v}dA = \frac{\overline{v_{x,d}}}{U_0}\frac{\Delta H}{\frac{1}{2}\rho U_0^2} = 2\frac{\overline{v_{x,d}}}{U_0}\frac{\Omega R}{U_0}\frac{\Gamma}{2\pi R U_0} \tag{8}$$

where $\overline{v_{x,d}}$ is the average axial velocity. The index d is used to indicate disc position, 0 the undisturbed flow far upstream and 1 for the fully developed wake far downstream. With $u_d = \overline{v_{x,d}}/U_0$, $\lambda = \Omega R/U_0$ and $q = \Gamma/(2\pi R U_0)$, (8) becomes:

$$C_p = 2q\lambda u_d. \tag{9}$$

The thrust T is obtained by integration of (3) on the disc area. In dimensionless form the thrust coefficient is $C_T = T/(\frac{1}{2}\rho U_0^2 A) = C_{T,\Delta H} + C_{T,\Delta v_\varphi}$ containing both terms on the right-hand side of (3). For $\delta \to 0$:

$$\left.\begin{array}{lcl} C_T & = & C_{T,\Delta H} + C_{T,\Delta v_\varphi} \\ C_{T,\Delta H} & = & 2\lambda q \\ C_{T,\Delta v_\varphi} & = & -q^2 \ln\left(\frac{R}{\delta}\right)^2 \end{array}\right\} \tag{10}$$

3. Momentum theory and numerical validation

The momentum theory as reported in [16] is unmodified, apart from the sign convention. An analytical solution is not available, but equation 29 of this paper gives an implicit expression of $u_1 = v_{x,1}/U_0$ in the independent variables λ and q:

$$\frac{(1-u_1)\,u_1^2 q^2}{1-2\lambda q - u_1^2} = \left(-q\lambda - \frac{1}{2}q^2\left(1 - \ln\left(\frac{q^2}{1-2\lambda q - u_1^2}\right)\right)\right), \tag{11}$$

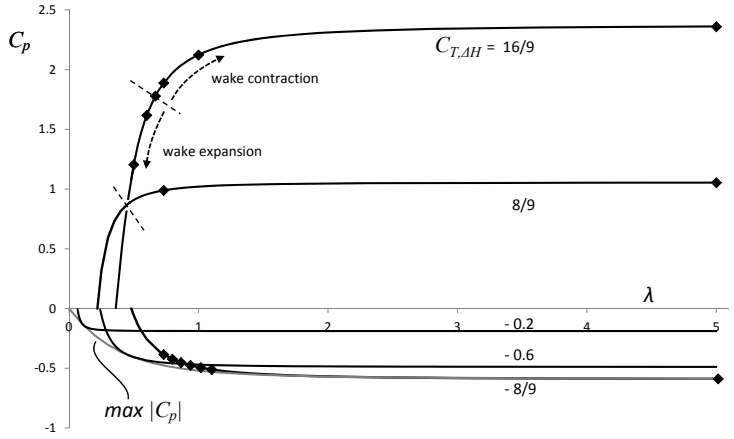

Figure 3. The Joukowsky momentum theory results (black lines), the maximum wind turbine $|C_p|$ (grey line) and the potential flow calculated results (♦)

in which the sign of q has changed as in [16] it was defined $-\Gamma/(2\pi R U_0)$. Equation (11) can be solved numerically for u_1. The wake expansion or contraction and, by continuity of mass, u_d follow from [16, eq. 28] and the velocity at the disc from [16, eq. 27].

Figure 3 shows results for several values of $C_{T,\Delta H}$. The potential flow calculations match the momentum theory values. Furthermore $|C_{P,max}(\lambda)|$ is shown, already presented in [16]. The figure indicates where propeller discs have an expanding wake for very low λ. This will be discussed in the next section. For $\lambda = 5$ the differences with the 1-D momentum theory are smaller than 0.7%, so the effect of the swirl is almost nill for $\lambda > 5$.

4. Performance of low λ wind turbine and propeller discs

4.1. Results of the momentum theory

Figures 4 and 5 show the solutions of (11), converted to u_d, and (9) for $0 \leq \lambda \leq 5$ and $-1 < C_{T,\Delta H} \leq +1$. Also indicated is the advance ratio $J = \pi/\lambda$ which is used for propellers. The front left sides show u_d respectively C_p for wind turbine discs, right behind for propeller discs. Several particularities can be observed, to be addressed in the next sections: for very low λ the velocity at propeller discs is < 1, so the wake expands as for wakes of energy extracting discs, and a minimum $\lambda > 0$ exists at which the velocity at the disc is 0, in both flow regimes.

Figure 6 shows the low λ regime with indications for wake expansion and contraction, and with indications for 3 pairs of flow states:

- wind turbine flow state `a` with $C_{T,\Delta H} = -8/9$, $\gamma_1/U_0 = -2/3$ and propeller flow state `b` with $C_{T,\Delta H} = 16/9$, $\gamma_1/U_0 = +2/3$, both with $\lambda = \infty$.
- flow states `c` and `d` with the same $C_{T,\Delta H}$ as `a` and `b` but for $\lambda = 1$.
- wind turbine flow state `a'` with $C_{T,\Delta H} = -0.7138, \lambda = \infty$ and propeller state `e` with $C_{T,\Delta H} = 16/9, \lambda = 0.5$, having equal flow deceleration.

Flow states `a` and `b` are without swirl, with `a` being analysed in [16]. The flow and pressure patterns are qualitatively similar to `c` and `d` and will not be shown.

4.2. Propeller discs with wake expansion

For low values of λ, the average axial velocity at the disc u_d and the power coefficient C_p deviate from Froude's result for both flow regimes: $u_d < \frac{1}{2}(u_1 + U_0)$. The explanation for this behaviour is the appearance in the momentum balance of the radial pressure distribution connected to the

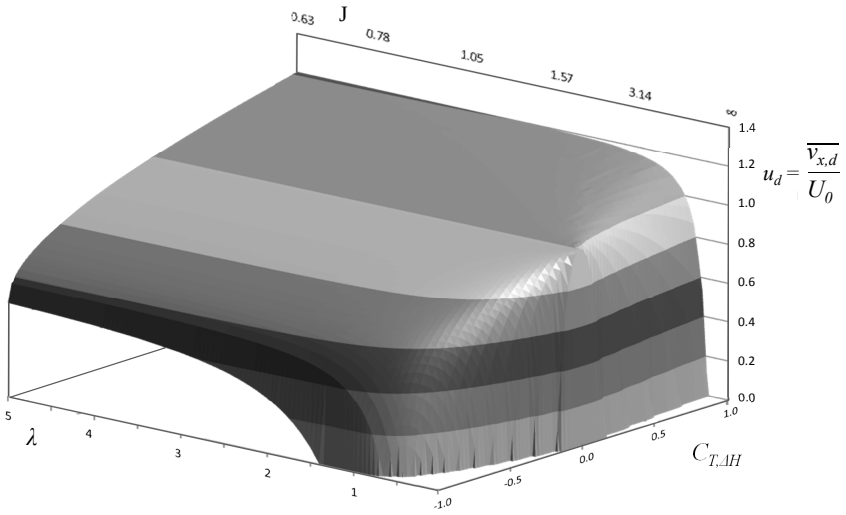

Figure 4. The axial velocity u_d at the disc for wind turbine discs ($C_{T,\Delta H} < 0$) and propeller ($C_{T,\Delta H} > 0$) for $0 \leq \lambda \leq 5$.

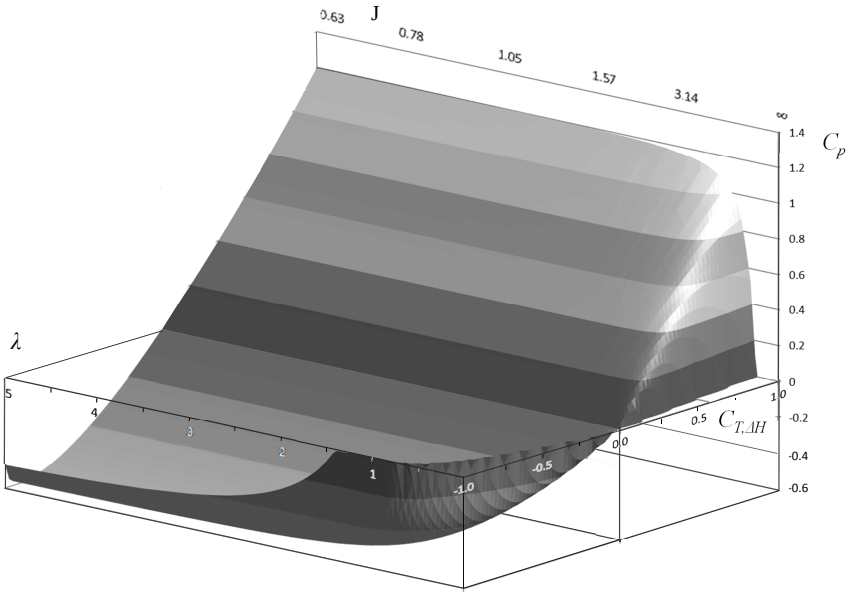

Figure 5. The power coefficient C_p for wind turbine discs ($C_{T,\Delta H} < 0$) and propeller ($C_{T,\Delta H} > 0$) for $0 \leq \lambda \leq 5$.

swirl, as is explained in [16]. The second term in the disc load equation (3) gives the contribution of the swirl related pressure to F_x. This contribution $-\frac{\rho}{2}(\Gamma/(2\pi r))^2$ is always < 0, while the first term $\Delta H < 0$ for wind turbine discs and > 0 for propeller discs. Consequently propeller flow states with a zero pressure jump at $r = R$ are possible. With (3) and (7) this gives the condition $\Omega R = -\frac{1}{2}v_\varphi$ or $\lambda = q/2$. The result is a flow with everywhere $v_x = U_0$, $v_r = 0$, and in the wake $v_\varphi = \Gamma/(2\pi r)$, see the line 'no wake deformation' in figure 6. The wake boundary consists of a cylindrical vortex sheet with constant radius R, having only axial vorticity across which $\Delta H = \frac{1}{2}(\Omega R)^2$. The swirl induces a lower pressure which is compensated by a higher pressure due to ΔH. As $u_d = 1$, the thrust and power coefficients are the same: $C_{T,\Delta H} = C_P = q^2 = 4\lambda^2$.

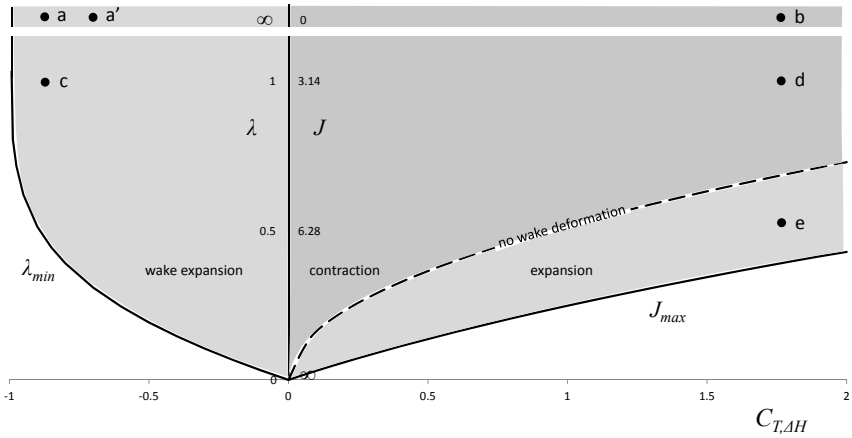

Figure 6. The operational regimes of an actuator disc: for negative $C_{T,\Delta H}$ energy is extracted from the flow, for positive $C_{T,\Delta H}$ energy is added. Details of the flow states indicated by `a` to `e` are explained in section 4.1

.

Both are positive as energy is supplied to the flow in the form of pressure.

For $\lambda > q/2$ and positive $C_{T,\Delta H}$ the wake contracts as expected for a disc in propeller mode. Figure 7 shows the streamlines and isobars of the disc flow with $\lambda = 1$ for $C_{T,\Delta H} = -8/9$ and $+16/9$ (flow states `c` and `d` in figure 6). The isobars in the wake show the pressure gradient due to the swirl. Figure 8 gives the meridian velocity v_m and axial velocity v_x at the disc, showing that v_m is constant for wind turbine flow `c`, but not for propeller flow `d`. This will be discussed further in the next section. Flow states `a` and `b`, not shown, have the same characteristics.

For $\lambda < q/2$ and positive $C_{T,\Delta H}$ the wake expands as for a disc in wind turbine mode. Flow states `a'` and `e`, indicated in figure 6, have the same far wake deceleration, see figure 9.

A complete blockage of the flow is possible as shown by $u_d = 0$ in figure 4, and the lines λ_{min} and J_{max} in figure 6.

4.3. The velocity at the disc

Figures 8 and 10 give velocity components at the disc, showing that the velocity in the meridian plane $v_m = \sqrt{v_x^2 + v_r^2}$ is constant for wind turbine discs. The same behaviour is found for all other values of $C_{T,\Delta H}$: v_m is uniform for all wind turbine flow states, and non-uniform for all propeller flow states. Upstream of the disc, so with $v_\varphi = 0$, Bernoulli's equation implies that $\partial p/\partial r = 0$ when $\partial v_m/\partial r = 0$. With the radial component of the equation of motion (2), upstream of the disc:

$$\frac{\partial p}{\partial r} = -\rho v_s \frac{\partial v_r}{\partial s}, \tag{12}$$

it is clear that for $\partial p/\partial r = 0$ at the upstream side of the disc, $\partial v_{r,d}/\partial s$ has to be 0.

This is checked by following a stream line passing the disc and observing the in- or decrease of v_r. This velocity component depends only on the position and strength of vorticity distribution γ_φ of the wake boundary. The following observations are made for a wind turbine disc flow:

(i) when the position of observation s^* travels from far upstream, s_0, to the disc position s_d, v_r increases due to the decreasing distance to the vorticity γ_φ in the wake boundary. The induction becomes stronger when the distance decreases, so $\partial v_r/\partial s > 0$.

(ii) following the streamline in the wake, so with $s^* > s_d$, two regions can be distinguished: the wake downstream of the disc up to the position of observation s^*, and the wake downstream

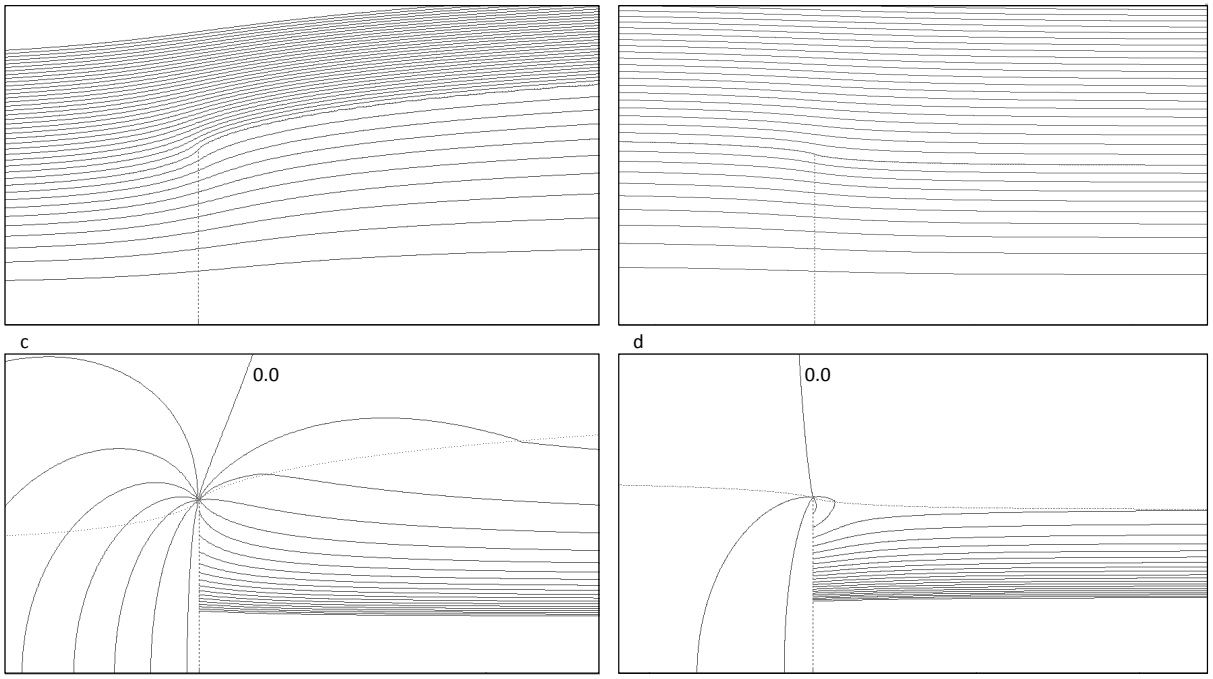

Figure 7. Flow states c and d with $\lambda = 1$ indicated in figure 6. Upper row: streamlines, lower row: isobars with $\Delta p = 0.1\Delta H$. Isobars close to the wake axis are not plotted.

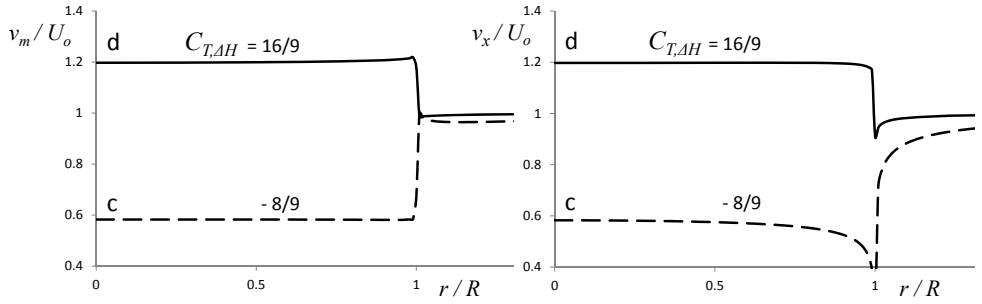

Figure 8. The velocity distribution at the disc for the flow states c and d with $\lambda = 1$. Left is shown the velocity in the meridian plane, $v_m = \sqrt{v_x^2 + v_r^2}$, right the axial velocity.

of s^*. The vorticity between s_d and s^* induces a negative v_r which increases for increasing s^*, so contributes to $\partial v_r/\partial s < 0$. The induction by the vorticity downstream of s^* does not change sign but becomes constant for large s^*, so $\partial v_r/\partial s \to 0$.

(iii) consequently $\partial v_r/\partial s = 0$ at the disc. With (12) $\partial p_d/\partial r = 0$ so v_m is constant.

However, this reasoning does not account for:

(iv) the variation in distance from the position of observation s^* to the most nearby vorticity due to the wake expansion, and similarly not for

(iiv) the variation in the strength γ_φ along the wake boundary sheet.

Apparently these additional aspects support the result that $\partial p/\partial r = 0$ for $C_{T,\Delta H} < 0$. However, repeating mutatis mutandis the line of arguments (i) to (iii) for positive $C_{T,\Delta H}$ leads to a similar conclusion that v_m should be constant, which is not true.

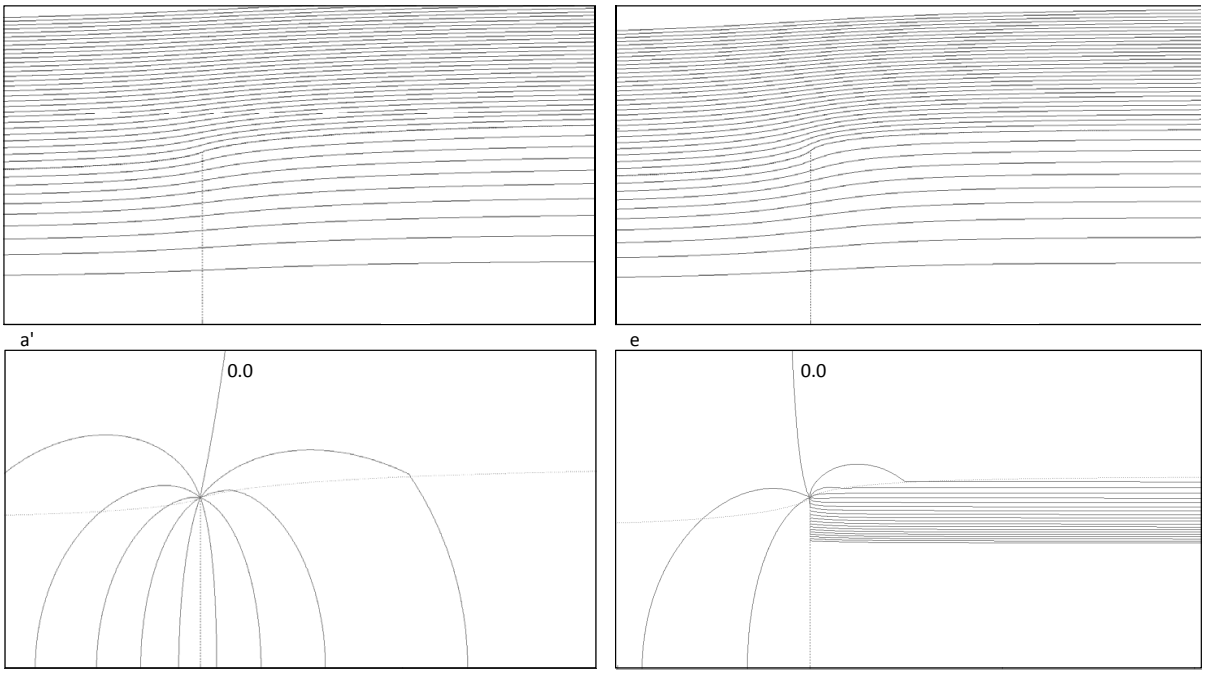

Figure 9. Flow states a' and e with the same $v_{x,wake}$, indicated in figure 6. Upper row: streamlines, lower row: isobars with $\Delta p = 0.1\Delta H$. Isobars close to the wake axis are not plotted.

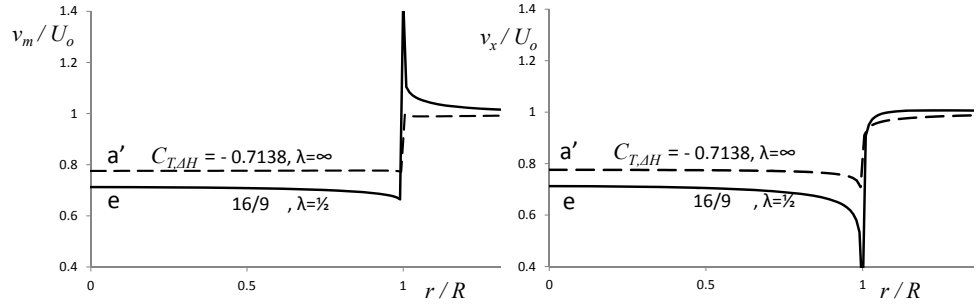

Figure 10. The velocity distribution at the disc for the flow states a' and e with the same $v_{x,1}$. Left is shown the velocity in the meridian plane, $v_m = \sqrt{v_x^2 + v_r^2}$, right the axial velocity.

Comparison of flow states c and d having $\lambda = 1$, see figure 7, with flow states a' and e having equal wake expansion, see figure 9, shows that wake expansion or contraction is not the decisive criterion for constant v_m, as propeller flow states e and d, having an expanding and contracting wake, show the same characteristics. The difference is in the distribution of $\gamma_\varphi(s)$ with s measured along the boundary of the stream tube. Figures 11 and 12 show the vorticity distribution of the flow states c - d and a' - e. In the propeller flow states $d\gamma_\varphi/ds$ does not change sign so there is no local maximum or minimum in γ_φ for $s > s_d$. In the wind turbine flow states such a local maximum (or minimum of $|\gamma_\varphi|$) exists. These observations hold for all flow states, including a and b without swirl, not shown. Apparently this local maximum in the distribution of γ_φ, together with arguments (i) to (iii), cause v_m to be uniform for wind turbine discs. A detailed analysis of the difference in induction nearby the disc edge by a vortex sheet with and without such a local maximum or minimum, has to show why $\partial v_r/\partial s = 0$ when such a maximum/minimum exists, and $\neq 0$ when this does not exist. This is left for future research.

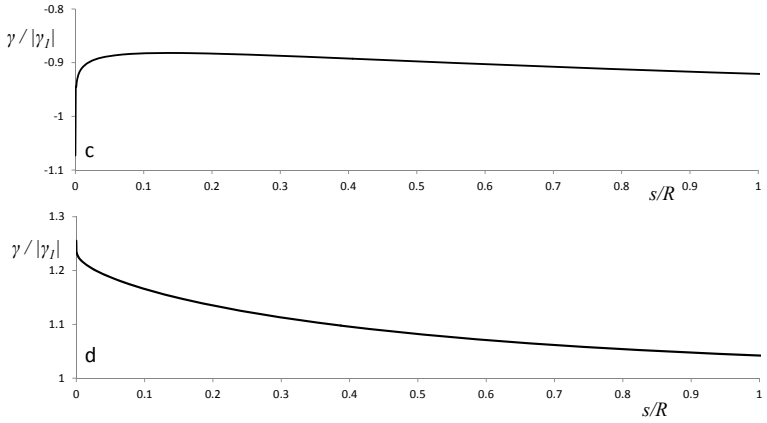

Figure 11. Strength of the vortex sheet as a function of the distance measured along the sheet, for the flow states `c` and `d` with $\lambda = 1$.

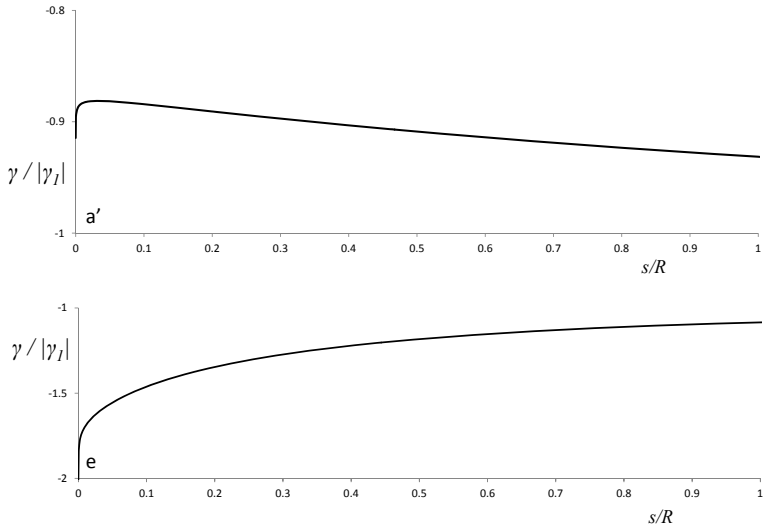

Figure 12. Strength of the vortex sheet as a function of the distance measured along the sheet, for the flow states `a'` and `e` with the same $v_{x,1}$. Note the different scale of the vertical axes.

5. Conclusions

The momentum theory plus the potential flow calculations have highlighted some aspects of actuator disc flows representing wind turbines and propellers with a constant circulation Γ:

- for $\lambda = \Omega R/U_0 = \Gamma/(4\pi R U_0)$ propeller discs have a wake without expansion or contraction,
- for lower λ propeller disc flows have an expanding wake, for higher λ a contracting wake,
- in the propeller as well as wind turbine flow regimes the velocity at the disc goes to 0 for very low λ, resulting in a minimum λ at which the flow is completely blocked,
- the meridian velocity $\sqrt{v_x^2 + v_r^2}$ is uniform for all wind turbine flow states, but non-uniform for all propeller flow states,
- this difference is due to an essential difference in the distribution of $\gamma_\varphi(s)$ along the wake boundary. For all propeller flows $d\gamma_\varphi/ds \neq 0$ for finite s, while for all wind turbine flows $d\gamma_\varphi/ds = 0$ at a short distance after the disc edge, showing a local maximum in γ_φ.

References

[1] H.A. Madsen, C. Bak, M. Døssing, R.F. Mikkelsen, and S. Øye. Validation and modification of the Blade Element Momentum theory based on comparisons with actuator disc simulations. *Wind Energy*, 13:373–389, 2010.
[2] R.F. Mikkelsen, S. Øye, J.N. Sørensen, H.A. Madsen, and W.Z. Shen. Analysis of Wake Expansion and Induction near Tip. In *Proceedings EWEC2009*, Marseille, 2009.
[3] A. Rosen and O. Gur. Novel Approach to Axisymmetric Actuator Disk Modeling. *AIAA Journal*, 46(11):2914–2925, nov 2008.
[4] P.R. Spalart. On the simple actuator disk. *Journal of Fluid Mechanics*, 494:399–405, nov 2003.
[5] J.N. Sørensen, W.Z. Shen, and X. Munduate. Analysis of wake states by a full field actuator disc model. *Wind Energy*, 88:73–88, 1998.
[6] M.D. Greenberg. Nonlinear actuator disk theory. *Zeitschrift für Flugwissenschaften*, 20:90–98, 1972.
[7] W. Haans, T. Sant, G.A.M. van Kuik, and G.J.W. van Bussel. HAWT Near-Wake Aerodynamics, Part I: Axial Flow Conditions. *Wind Energy*, 11:245–264, 2008.
[8] D. Medici and P.H. Alfredsson. Measurements on a wind turbine wake: 3D effects and bluff body vortex shedding. *Wind Energy*, 9:219–236, 2006.
[9] J.G. Leishman. *Principles of Helicopter Aerodynamics, 2nd edition.* Cambridge University Press, 2006.
[10] G.A.M. van Kuik. Experimental verification of an improved actuator disc concept. In *15th European Rotorcraft Forum*, Amsterdam, 1989.
[11] S. Wilmshurst, A.J.F. Metherell, D.M.A. Wilson, D.J. Milborrow, and J.N. Ross. Wind turbine rotor performance in the high thrust region. In *Sixth BWEA Conference*, 1984.
[12] H.B. Anderson, D.J. Mi1borrow, and J.N. Ross. Performance and wake measurements on a 3 m diameter horizontal axis wind turbine rotor. In *Proc. 4th Int1. Symposium on Wind Energy Systems. Stockholm, BHRA*, 1982.
[13] E.A. Parra, K. Boorsma, J.G. Schepers, and H. Snel. Momentum considerations on the New MEXICO experiment. *Journal of Physics: Conference Series*, 753(Torque):072001, 2016.
[14] L.E.M. Lignarolo, C.S. Ferreira, and G.J.W. van Bussel. Experimental comparison of a wind turbine and of an actuator disc wake. *Journal of Renewable and Sustainable Energy*, 8(023301):1–26, 2016.
[15] G.A.M. van Kuik and L.E.M. Lignarolo. Potential flow solutions for energy extracting actuator disc flows. *Wind Energy*, 19:1391–1406, 2016.
[16] G.A.M. van Kuik. Joukowsky actuator disc momentum theory. *Wind Energy Science*, 2:307–316, 2017.